ELSEVIER

Ceramics International 28 (2002) 899–905

CERAMICS INTERNATIONAL

www.elsevier.com/locate/ceramint

Microstructural evolution and mechanical performances of SiC/SiC composites by polymer impregnation/microwave pyrolysis (PIMP) process

S.M. Dong[a,*], Y. Katoh[a], A. Kohyama[a], S.T. Schwab[b], L.L. Snead[c]

[a]*CREST-ACE, JST and Institute of Advanced Energy, Kyoto University, Gokasho, Uji, Kyoto 611-0011, Japan*
[b]*Thor Technologies, Inc. 7600 Jefferson NE, Suite 9-115, Albuquerque, NM 87109, USA*
[c]*Metals and Ceramic Division, Oak Ridge National Laboratory, PO Box 2008, Oak Ridge, TN 37831-6087, USA*

Received 8 January 2002; received in revised form 9 February 2002; accepted 26 March 2002

Abstract

SiC/SiC composites were prepared by polymer impregnation/microwave pyrolysis (PIMP) process, and their microstructural evolution and the mechanical performances were characterized. Using non-coated Tyranno SA fiber preforms as reinforcement and impregnation with only allylperhydropolycarbosilane (AHPCS) into the preforms, Tyranno SA/SiC composite (TSA/SiC) with higher density was obtained. While using carbon-coated Tyranno SA fiber preforms, Tyranno SA/C/SiC composite (TSA/C/SiC) with lower density were also fabricated. In this composite, SiC particulate was loaded with polymer precursor (AHPCS) in the first cycle impregnation. Microstructural observation revealed that pore and crack formation was affected by processing conditions. Bending strength was also dependent on the microstructural evolution of the samples. In TSA/SiC composite, relatively strong interfaces contribute to effective load transfer so that higher bending strength could be reached. In the TSA/C/SiC composite, weak interfaces provide a relatively lower strength. Meanwhile, different microstructural evolution and interfacial properties of the composites lead to the variation of the fracture behaviors.

Keywords: B. Composites; B. Microstructure-final; C. Mechanical properties; D. SiC; PIMP

1. Introduction

SiC/SiC composite is a well-known material promising for high temperature structural applications because of its intrinsic thermal stability and excellent mechanical properties. Polymer impregnation and pyrolysis (PIP) processing is considered to be an effective manufacturing technique for preparing high performance SiC/SiC composite. Since the shapes of the impregnated parts can be varied intentionally, it will be widely applied to the complex-shaped components [1]. For matrix formation, many kinds of polymer precursors have been investigated and the details of polymer to ceramic conversion, microstructural development as well as some physical and mechanical properties have been studied [1–5]. However, because of the lengthy pyrolysis cycles, much time is required in conventional PIP process to produce a dense component, resulting in high-cost for even simple shapes.

Fast heating, techniques such as microwave or laser heating are now being applied for ceramic fabrication or polymer pyrolysis process [6–8]. These novel processing techniques provide a time and energy saving way for ceramic preparation. Although those works are still on the fundamental stage, promising features have been demonstrated for ceramics development such as short processing time, uniformity of the products as well as tailoring particular design requirements of the materials. Meanwhile, high frequency microwave radiation can also be applied to induce the polymer-to-ceramic conversion process, and can induce very high temperature in irradiated parts in just minutes [9].

The aim of the present study is to characterize the microstructural evolution of SiC/SiC composites

* Corresponding author. Tel.: +81-774-38-3465; fax: +81-774-38-3467.
E-mail address: sm-dong@iae.kyoto-u.ac.jp (S.M. Dong).

0272-8842/02/$22.00 © 2002 Published by Elsevier Science Ltd and Techna S.r.l.
PII: S0272-8842(02)00071-8

fabricated by polymer impregnation/microwave pyrolysis (PIMP) process using 2 D woven Tyranno SA fiber preforms as the reinforcement. The effects of fiber coating and particulate loading during first cycle impregnation on fiber/matrix interaction and mechanical behaviors are also evaluated.

2. Experimental procedure

2.1. Materials

Polymer precursor used for matrix formation was allylperhydropolycarbosilane (AHPCS), which is regarded as a polymer precursor of high ceramic yield [10]. Since this polymer precursor is very sensitive to the ambient atmosphere, it was handled under strictly anhydrous and anaerobic environment to minimize the potential for oxygen contamination. The maximum pyrolysis temperature obtained by microwave irradiation at 37 GHz was approximately 1100 °C. The heating time in each cycle was less than 5 min. Detailed processing technique has been described in literature [9].

Two kinds of SiC/SiC composites were prepared according to PIMP process. The first one is non-coated Tyranno SA fiber (Ube Industries Ltd., Japan) reinforced SiC composite (TSA/SiC). During impregnation and pyrolysis, the polymer precursor was used unloaded (no SiC particulate). Eight cycles of impregnation/pyrolysis processing were performed. The second is carbon coated Tyranno SA fiber reinforced SiC composite (TSA/C/SiC). In this composite, β-SiC particles (with an average diameter of 0.6 μm) were added to the precursor in the first cycle of impregnation and then the material was submitted to microwave pyrolysis. This first cycle was followed by five cycles of PIMP with unloaded AHPCS. In the first PIMP cycle, polymer to filler (SiC) ratio was 50% to 50% by weight. All fiber reinforcements used in this experiment were 2-D woven fabrics, and fiber volume fraction of the composites was about 30–35 vol.%. The fiber volume fraction for composite TSA/SiC is slightly higher than that in the second material. Typical properties of Tyranno SA fiber used in this experiment are listed in Table 1.

2.2. Microstructural observation

Optical microscopy and scanning electron microscopy (SEM) were conducted on the polished cross-section of all the samples. Fracture surface of each sample after bending test was also observed by SEM to determine the fracture behavior. Microstructural evolution of the AHPCS derived matrix after PIMP process was characterized by transmission electron microscopy (TEM). The thin film was prepared by the focused ion beam (FIB) method.

2.3. Physical and mechanical measurements

All PIMP samples were cut and ground into nearly 4×2×20 mm rectangular bars to perform three-point bending test at room temperature with an Instron 5581 test machine. The cross-head speed was 0.5 mm/min and the span was 18 mm. During bending test, the fracture behavior of the bars was in situ recorded by optical microscope camera. The bulk density of the composites was measured by Archimedes's method.

Push-out and push-back tests were performed on thin slices of each sample to evaluate the interfacial debonding strength (IDS) and interfacial frictional stress (IFS), respectively, using a load controlled micro-indentation testing system. Those slices were double-face polished, their thickness being less than 100 μm to allow the fibers to be pushed out. During this test, the slices were set on a tungsten carbide holder with a 50 μm width groove, and the load was applied on a single fiber end above the groove using a triangle diamond indenter. The maximum load was 1N and this load was modified according to the value of IDS and IFS. The interfacial displacement rate was 0.2 μm/s. After push-out test, the protruding fibers were firstly observed by SEM, and then push-back test was conducted on those protruding fibers.

3. Results and disscussion

3.1. Microstructural evolution

By contrast to the conventional polymer impregnation and pyrolysis (PIP) technique, the PIMP only requires very short pyrolysis time. Because the polymer to ceramic conversion is a complex process, such very short pyrolysis duration might affect the evolution of microstructure. Fig. 1 shows a typical SEM micrograph of the polished cross-section. Actually, well-consolidated parts dominate the cross section area. Some isolated large pores could be observed in inter-bundle

Table 1
Properties of Tyranno SA fibers (Grade II)

SiC fiber	C/Si atomic ratio	Diameter (μm)	Density (g/cm^3)	Filaments/yarn	Tensile strength (GPa)	Elastic modulus (GPa)	Elongation%
Tyranno SA	1.08	10	3.02	800	2.8	420	0.7

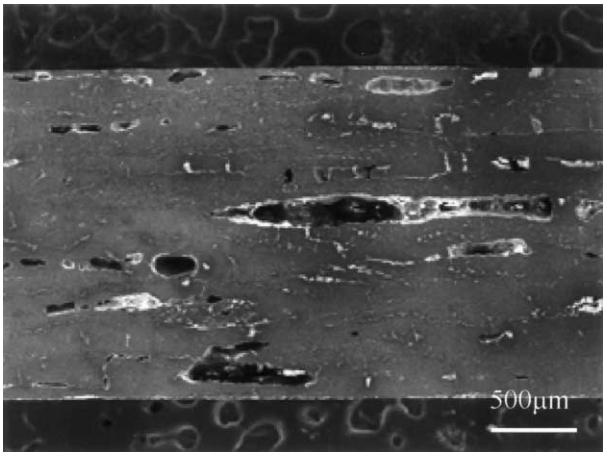

Fig. 1. Typical SEM micrograph on the polished cross-section of the composite TSA/SiC.

areas and inter-layers. This is also the typically observed phenomenon in conventional PIP prepared samples. Further observation of the intra-bundle and inter-bundle matrix formation was conducted by optical microscopy on the polished cross-section, as shown in Fig. 2. Dense intra-bundle matrix can be identified. Meanwhile, microcracks still remained but more extensively in the TSA/C/SiC composite. In this composite, relatively large amount of matrix formed in both intra-bundle and inter-bundle areas (Fig. 2b), indicating that the infiltration efficiency was high when particulates were loaded in the first-cycle of impregnation. In composite TSA/SiC (using non-coated Tyranno SA fiber preforms as reinforcement and without particulate loading during impregnation), intra-bundle fibers and fiber layers were tightly bonded together. Only thin inter-layer matrix could be evidenced, as shown by arrow in Fig. 2a. These results might be ascribed to low mass inclusion (without the addition of SiC particles) and large volume shrinkage by the pure polymer precursor during the pyrolysis process.

Microstructure of intra-bundle matrix is shown in Fig. 3. In composite TSA/SiC, as the PIMP process progresses, the matrix became dense. Meanwhile, the initially formed matrix around fibers could also be identified in some areas. The following cycles of PIMP left a clear profile in intra-bundle matrix. Even in this case, the matrix relatively maintained the uniformity around fibers. However, some debonding between fibers and matrix could be observed. In TSA/C/SiC composite, matrix seems not to be dense even though large amounts of intra-bundle matrix and inter-bundle matrix were effectively formed in the first cycle impregnation, and the particles were not strongly bonded together at the present PIMP temperature. This "porous" matrix might be ascribed to the difficulty for achieving effective polymer impregnation after the matrix was formed in the first cycle impregnation. Generally, during PIMP process, the micropores left in the matrix would decrease gradually in size when PIMP cycles proceeded and then hindered further polymer impregnation. When the pores were small enough, the viscous polymer precursor could not be effectively impregnated into the consolidated body. At this time, the process should be stopped. With particulate loading, the inter-bundle and intra-bundle spaces were relatively easier to be filled. After few cycles of PIMP, the remaining porosity, especially the open porosity on the outer surface of the composites was greatly lowered, making the impregnation more difficult. Since both of the composite densification and matrix strengthening are highly dependent on the polymer impregnation and pyrolysis, insufficient impregnation of polymer precursor implies that the matrix might not be strongly bonded. In the TSA/C/SiC composite, polymer impregnation was stopped after six cycles of PIMP, while for TSA/SiC, eight cycles could be performed.

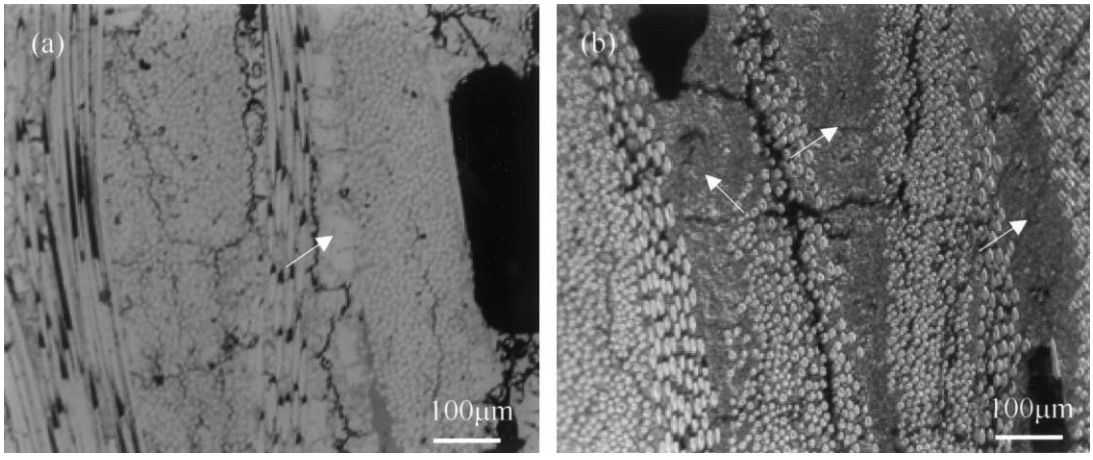

Fig. 2. Optical photographs of the polished cross-section of the composites showing the intra-bundle and inter-bundle matrix formation and the cracks propagation: (a) TSA/SiC, (b) TSA/C/SiC.

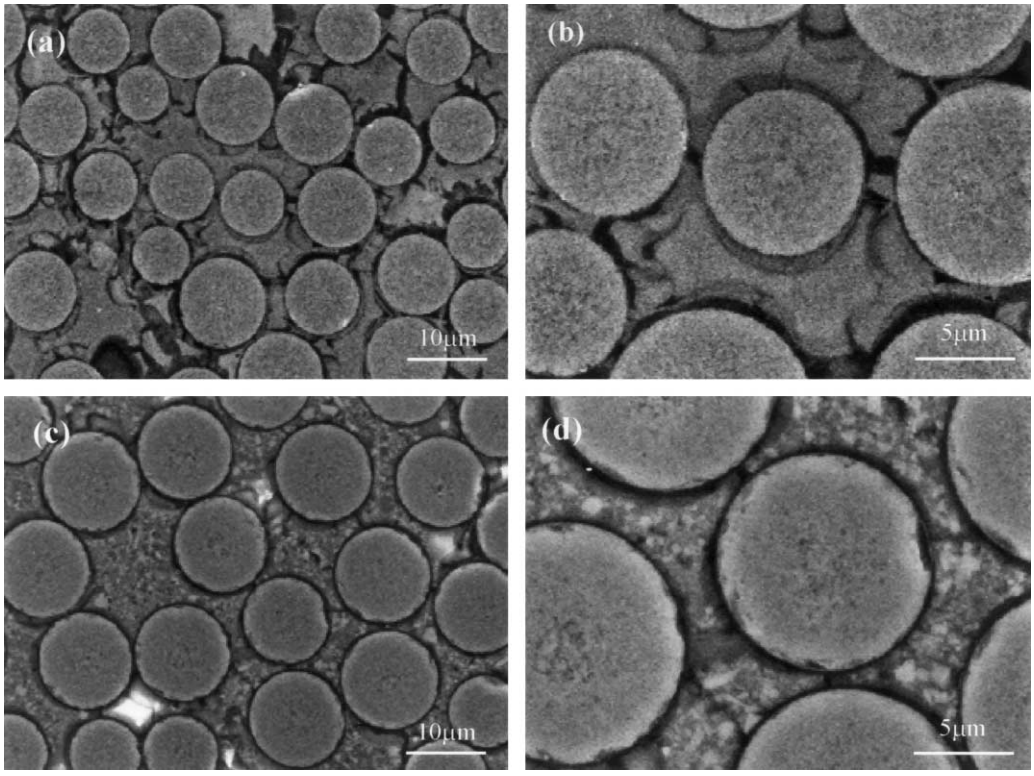

Fig. 3. Comparison of the microstructural evolution of the PIMP composites: (a), (b) TSA/SiC; (c), (d) TSA/C/SiC.

The microstructure of the composites at a higher magnification is shown in Fig. 3b and d. Some microcracks can be observed around the fibers. Even though large amounts of inter-bundle and intra-bundle matrix were effectively formed in TSA/C/SiC composite, the intra-bundle matrix seems to be loosely consolidated. This feature could be distinguished from the inter-bundle matrix areas.

TEM observation of the matrix from AHPCS precursor is shown in Fig. 4. It can be evidenced from the SAD-pattern that the matrix is completely amorphous, probably due to the very short pyrolysis time and low pyrolysis temperature (around 1100 °C).

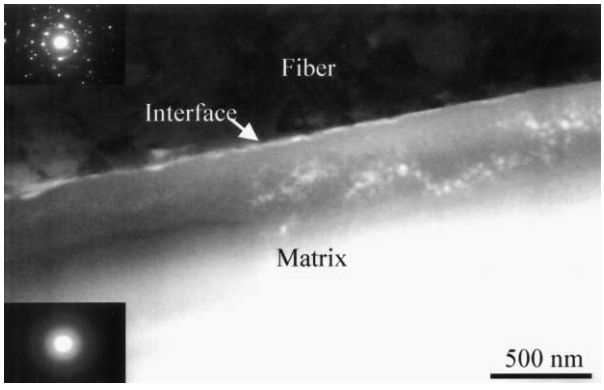

Fig. 4. TEM image and SAD-pattern (inset) of the composite TSA/SiC showing the formation of non-crystallized matrix.

3.2. Physical and mechanical properties

Table 2 lists some physical and mechanical properties of the composites. Bulk density of TSA/SiC composite is relatively high (2.51 g/cm^3) compared to that (2.30 g/cm^3) for TSA/C/SiC composite. In composite TSA/SiC, as discussed in the previous section, intra-bundle matrix was gradually grown around the fibers when increasing the number of impregnation cycles. After eight cycles PIMP process, polymer derived matrix was formed in the intra-bundle and inter-bundle areas. Although some big pores inevitably existed, the density of TSA/SiC could still reach 2.51 g/cm^3. In the TSA/C/SiC composite, the formation of relatively loose microstructure with the inclusion of SiC particulates and the less efficient impregnation cycles might explain the lower density.

Bending test results indicate that higher strength could be obtained for the composite with higher density (TSA/SiC). The average strength of this composite is over 400 MPa. While for the composites with lower density, strength is at a lower level.

To better understand the interaction between fibers and matrix, push-out and push-back tests were conducted on each composite. Typical curves are shown in Fig. 5a. Protruding fiber is also demonstrated as an example in Fig. 5b. In TSA/C/SiC, debonding mainly occurred in the fiber/carbon interface during push-out test. In Fig. 5, P_o represents the push-out load, which

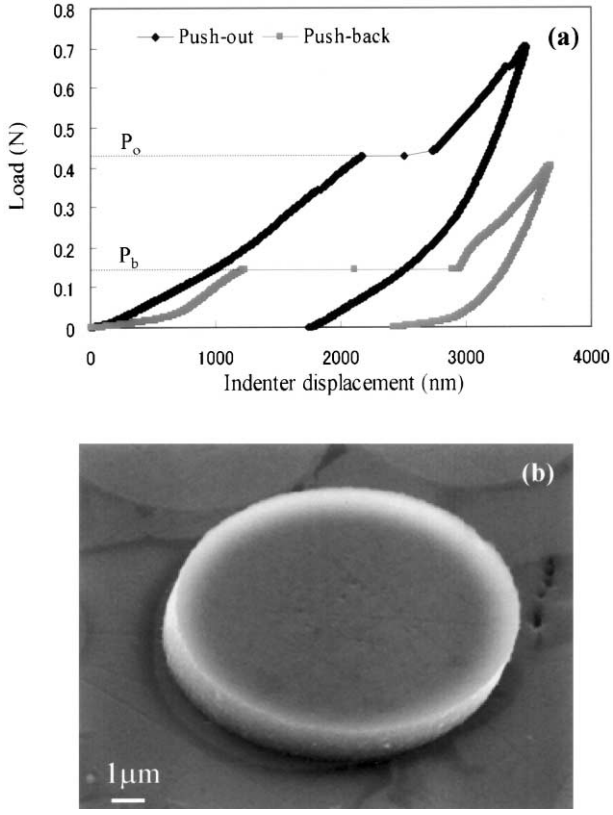

Fig. 5. Typical single fiber push-out and push back load/displacement curves (a), and SEM micrographs of the protruding fibers after single fiber push-out test (b) for composite TSA/SiC.

means the load for fiber debonding and sliding as well as the contributions from fiber elastic/plastic deformation and Poisson expansion effects [11]. It is used in this study for estimating the interfacial debonding strength, IDS via the formula:

$$\mathrm{IDS} = P_o/\pi Dt \tag{1}$$

where D and t are the fiber diameter and the specimen thickness of the slice for push-out and push-back test. The same formula was also used for determining the interfacial frictional stress (IFS), where P_o was substituted by P_b, which is mainly used to initiate the sliding of the debonded fiber.

From the calculated results listed in Table 2, it can be observed that a relatively strong interface is present in TSA/SiC. Although microcracks around some fibers have been formed, the average IDS still reaches 161.1 MPa. In composites TSA/C/SiC, relatively weak interfaces were formed. The data for interfacial frictional stress reveal the same trend as that of the IDS. TSA/SiC composite also shows a higher IFS value. However, it should be mentioned that, debonding between fibers and matrix could still be realized under certain load during push-out test in TSA/SiC although the matrix and fibers were directly bonded during the PIMP process.

Table 2
Physical and mechanical properties of the composites

Composites	TSA/SiC	TSA/C/SiC
Bulk density (g/cm^3)	2.51±0.02	2.30±0.04
Flexural strength (MPa)	402.4±35.9	258.7±26.0
Interfacial debonding strength (MPa)	161.1±31.6	61.5±17.8
Interfacial frictional stress (MPa)	56.9±18.2	32.8±10.1
Modulus of elasticity (GPa)	102.0±5.3	49.7±4.8

The differences of interfacial debonding strength and interfacial frictional stress might be ascribed to the interaction between fibers and matrix [12–15]. Generally, the radial stress on the fibers can be described by [16],

$$\sigma_r^N = \sigma_r^T + \sigma_r^R + \sigma_r^P \tag{2}$$

where σ_r^T is radial thermal residual stress given by

$$\sigma_r^T = \kappa\left(\alpha_m^r - \alpha_f^r\right)\Delta T \tag{3}$$

σ_r^R is fiber surface roughness induced radial misfit stress given by

$$\sigma_r^R = \kappa\left(\frac{\delta}{R_f}\right) \tag{4}$$

$$\kappa = \frac{\omega E_m E_f}{E_m(1-\upsilon_f) + E_f(1+\upsilon_m)} \tag{5}$$

σ_r^P is the radial stress induced by Poisson's effect. α_m^r And α_f^r are the thermal expansion coefficients of the fiber and matrix in the radial direction. ΔT is the temperature difference between composite fabrication temperature (1373 K) and room temperature (298 K), at which the push-out and push-back test were conducted. E_f, E_m, υ_f^r and υ_m^r are Young's moduli and Poisson's ratios of the fiber and matrix. δ Is the fiber surface roughness. In this experiment, fiber surface roughness profiles for Tyranno SA fiber was examined by an optical interferometric microscope, Micromap™, with a resolution of less than 1 nm in Z-direction, and δ was determined to be 3.74. ω Is a factor for the effect of fiber volume fraction in the composites. Here, σ_r^P and ω are simply assumed to be zero and 1, respectively. Since the Tyranno SA is well crystallized and near stoichiometric [17], their thermal expansion coefficients can be assumed to be similar as those of the sintered SiC monolithic ceramics (about 4.0×10^{-6}/K) [18]. For the polymer derived matrix, thermal expansion coefficient can be simply assumed to be $3.0–3.5\times10^{-6}$/K (similar to that of a Si–C[–O] amorphous phase) [18,19]. Based on those assumptions, the radial stress on the fibers in the composites can be roughly estimated using Eqs. (2)–(5).

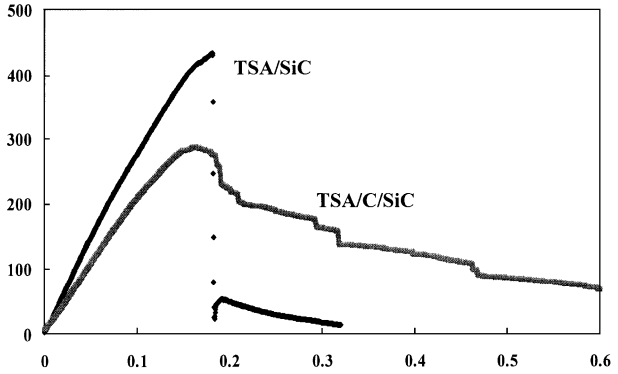

Fig. 6. Stress/displacement curves of the composites.

Because $\alpha_m^r < \alpha_f^r$ in the composites, a radial tension stress was induced to the fiber/matrix interface by thermal mismatch. This might explain the occurrence of some fiber/matrix debonding as indicated in Fig. 3. For TSA/C/SiC, the carbon coating will simultaneously affect the interfacial stresses [17]. The radial tension stress can weaken the fiber/matrix interfacial bonding and significantly reduce the applied load during the fiber push-out and push-back [13]. This effect might be beneficial for the composite TSA/SiC to prevent a too strong fiber/matrix bonding in the case of no coating applied.

The roughness induced radial stress will highly contribute to the IFS, as analyzed in literature [13,14,16]. In the present study, Tyranno SA fiber is confirmed to have a rather rough surface so that the contribution to the IFS is high. This characteristic will finally affect the mechanical properties of the composites.

Typical stress/displacement curves obtained from bending test are shown in Fig. 6. TSA/SiC composite displays not only higher strength but also a high modulus of elasticity, as summarized in Table 2. These mechanical properties may be attributed to the densely formed matrix and the strong interface between fibers and matrix. The strong interface is beneficial for the load transfer from matrix to fibers so that higher strength could be obtained [20,21]. Load/displacement curve of TSA/C/SiC demonstrates a different behavior with respect to the TSA/SiC composite. After reaching the maximum value, the load decreases gradually indicating a pseudo-ductile fracture behavior. This characteristic might be ascribed to the relatively loose matrix and weak interface also, providing the lower elastic modulus. Even though the weak interface is benefitial for the crack bridging and fiber pull-out, it is simultaneously detrimental for strength because of the low load transfer ability from matrix to fibers through the weak interface.

3.3. Fracture behaviors of the composites

Fig. 7 shows the fracture surfaces of the composites. For TSA/SiC, short fiber pull-out is apparent (Fig. 7a). Although polymer derived matrix directly bonded with fibers, this bonding was weakened by the tensile effect induced by thermal mismatch so that the debonding between fibers and matrix became possible. In situ observation during bending test indicated that crack propagated nearly parallel to the direction of the load applied. No delamination along fiber layers could be found, and the tensile fracture is predominant. TSA/C/SiC composite demonstrates long fiber pull-out, as shown in Fig. 7b. The in situ observation indicated that the fracture propagated in two directions: one is nearly parallel to that of the applied load and another is nearly perpendicular to that of the applied load. It means that both tensile fracture and shear fracture exist in this composite.

The dense matrix in the TSA/SiC composite would prevent delamination along the fiber layers. The strong bonding was beneficial for load transfer from matrix to fibers and simultaneously limited the fibers pull-out. In TSA/C/SiC composite, since the density is relatively low and the matrix was loosely formed during PIMP process, cracks easily propagate along the weak region. Meanwhile, the weak load transfer between matrix and fibers in this composite allows the long fibers pull-out.

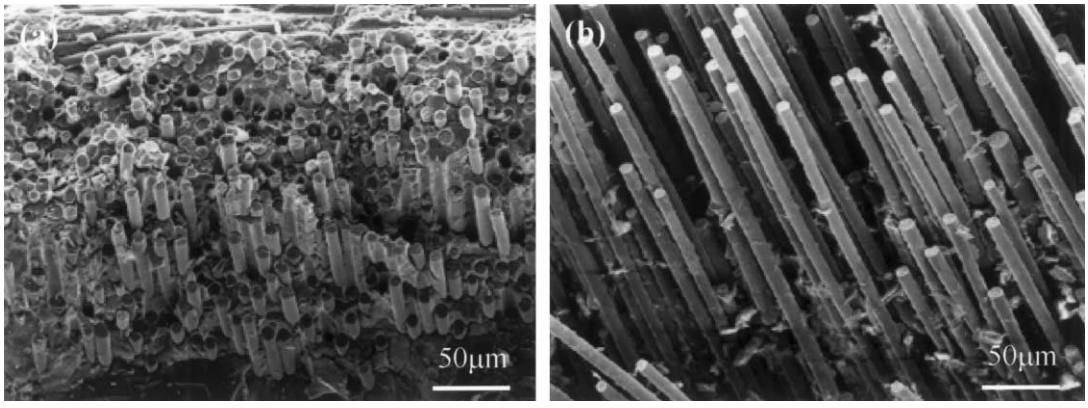

Fig. 7. SEM micrographs of the fracture surface after bending test showing the different behaviors of the PIMP composites: (a) TSA/SiC, (b) TSA/C/SiC.

4. Conclusions

The composite without carbon coating and particulate loading demonstrates higher density and flexural strength. In this composite, a relative strong interface between matrix and fibers could be formed. The strong interface can provide the high ability for load transfer from matrix to fibers and prevent the delamination of the fiber layers.

The composites with carbon coating and particulate loading present a relatively lower density and flexural strength. This composite has a relatively weak interface and shows long fiber pull-out. During bending test, shear fracture occurred leading to the delamination along the interlayers. With the adjustment of the filler addition in the impregnated polymer precursor and fiber coating, interfacial properties could be changed. This implies that the fracture behaviors can be further modified to fit the requirement for preparing strong composites and/or tough composites by PIMP process.

Acknowledgements

This work was conducted at the Institute of the Advanced Energy, Kyoto University, as a part of Core Research for Evolutional Science and Technology (CREST) program administered by Japan Science and Technology Corporation (JST).

References

[1] K. Sato, A. Tezuka, O. Funayama, T. Isoda, Y. Terada, S. Kato, M. Iwata, Fabrication and pressure testing of a gas-turbine component manufactured by a preceramic-polymer-impregnation method, Comp. Sci. Tech. 59 (1999) 853–859.

[2] G.D. Soraru, F. Babonneau, J.D. Mackenzie, Structural evolutions from polycarbosilane to SiC ceramics, J. Mater. Sci. 25 (1990) 3886–3893.

[3] M.J. Wild, P. Buhler, On the phase composition of polymethylsiloxane derived ceramics, J. Mater. Sci. 33 (1998) 5441–5444.

[4] G. Ziegler, I. Richter, D. Suttor, Fiber-reinforced composites with polymer-derived matrix: processing, matrix formation and properties, Composites A30 (1999) 411–417.

[5] M. Kotani, A. Kohyama, K. Okamuram, T. Inoue, Fabrication of high performance SiC/SiC composite by polymer impregnation and pyrolysis method, Ceram. Eng. Sci. Proc. 20 (1999) 309–316.

[6] H.H. Streckert, K.P. Norton, J.D. Katz, J.O. Freim, Microwave densification of electrophoretically infiltrated silicon carbide composite, J. Mater. Sci. 32 (1997) 6429–6433.

[7] B.G. Ravi, V. Praveen, M. Panneer Sevam, K.J. Rao, Microwave-assisted preparation and sintering of mullite and mullite-zirconia composites from metal organics, Mater. Res. Bull. 33 (1998) 1527–1536.

[8] K. Jakubenas, H.L. Marcus, Silicon carbide from laser pyrolysis of polycarbosilane, J. Am. Ceram. Soc. 78 (1995) 2263–2266.

[9] S.T. Schwab, P.F. Fleig, T. Chen, J.D. Katz, T.W. Hardek, K.W. Buesking, Enhanced PIP processing of SiC/SiC for fusion applications, in: Proceeding 3rd IEA International Workshop on SiC/SiC Ceramic Composites for Fusion Applications, 1998.

[10] L.V. Interrante, C.W. Whitmarsh, W. Sherwood, H.J. Wu, R. Lewis, G. Maciel, High yield polycarbosilane precursors to stoichiometric SiC: synthesis, pyrolysis and application, Mater. Res. Soc. Symp. Proc. 346 (1994) 593–603.

[11] T. Hinoki, W. Yang, T. Nozawa, T. Shibayama, Y. Katoh, A. Kohyama, Improvement of mechanical properties of SiC/SiC composites by various surface treatments of fibers, J. Nucl. Mater. 289 (2001) 23–29.

[12] R.J. Kerans, R.S. Hay, N.J. Pagano, T.A. Parthasarathy, The role of the fiber–matrix interface in ceramic composites, Ceram. Bull. 68 (1989) 429–442.

[13] P.D. Jero, R.J. Kerans, T.A. Parthasarathy, Effect of interfacial roughness on the frictional stress measured using pushout tests, J. Am. Ceram. Soc. 74 (1991) 2793–2801.

[14] T.A. Parthasarathy, D.B. Marshall, R.J. Kerans, Analysis of the effect of interfacial roughness of fiber debonding and sliding in brittle matrix composites, Acta Metall. Mater. 42 (1994) 3773–3784.

[15] F. Rebillat, J. Lamon, R. Naslain, E.L. Curzio, M.K. Ferber, T.M. Besmann, Properties of multilayered interphases in SiC/SiC chemical-vapor-infiltrated composites with "weak" and "strong" interfaces, J. Am. Ceram. Soc. 81 (1998) 965–978.

[16] Y. Tanaka, Y. Kagawa, Y.F. Liu, C. Masuda, Interface damage mechanism during high temperature fatigue test in SiC fiber-reinforced Ti alloy matrix composite, Mater. Sci. Eng. A314 (2001) 110–117.

[17] S.M. Dong, G. Chollon, C. Labrugere, M. Lahaye, A. Guette, R. Naslain, D.L. Jiang, Characterization of some advanced SiC-based ceramic fibers, J. Mater. Sci. 36 (2001) 2371–2381.

[18] J.L. Bobet, J. Lamon, Thermal residual stress in ceramic matrix composites—I. Axisymmetrical model and finite element analysis, Acta Metall. Mater. 43 (1995) 2241–2253.

[19] C.A. Hasegawa, A. Kohyama, R.J. Jones, L.L. Snead, B. Riccardi, P. Fenici, Critical issues and current status of SiC/SiC composites for fusion, J. Nucl. Mater. 283–287 (2000) 128–137.

[20] F. Rebillat, J. Lamon, A. Guette, The concept of a strong interface applied to SiC/SiC composites with a BN interphase, Acta Mater. 48 (2000) 4609–4618.

[21] F. Rebillat, J. Lamon, R. Naslain, E.L. Curzio, M.K. Ferber, T.M. Besmann, Interfacial bond strength in SiC/SiC composite materials, as studied by single-fiber push-out tests, J. Am. Ceram. Soc. 81 (1998) 2315–2326.